Ultracompact object within a nonlocal Tolman VII model

B. N. Jayawiguna,[*] I. Prasetyo,[†] A. Sulaksono,[‡] and H. S. Ramadhan[§]
Departemen Fisika, FMIPA, Universitas Indonesia, Depok 16424, Indonesia

(Received 27 July 2022; accepted 18 October 2022; published 10 November 2022)

Tolman VII (TVII) is an analytical model for the nonrotating perfect fluid sphere with a simple quadratic density profile where its value is zero at the surface and a finite critical density value at the center. Therefore, compared to another analytical model like the constant density star, TVII is more realistic. Except for the dominant energy condition (DEC), which is violated in the region near the star's center, the TVII satisfies all energy conditions. However, the causal condition is also violated for $\mathcal{C} > 0.26$, and the maximum compactness of the TVII is restricted, i.e., $\mathcal{C}_{\max} \approx 0.38$. Here, we investigate the impacts of nonlocal gravity on the properties of the star of TVII within the range of the compactness of an ultracompact star ($0.33 \leq \mathcal{C} \leq 0.44$). This nonlocal gravity version of TVII (NGTVII) is parametrized by the nonlocal parameters ($\tilde{\beta}$) and the compactness ($\mathcal{C}$). We have found that NGTVII can reach $\mathcal{C}_{\max} = 0.43$ with $\tilde{\beta}_{\max} = 3$ which is significantly more compact than TVII. The nonlocal density and pressure profile differs from the TVII, depending on the stars' compactness and nonlocal parameter. We have also found that for the relatively small value of $\tilde{\beta}$ and the compactness, i.e., $\mathcal{C} \lesssim 0.31$, the causality condition and the DEC are not violated. We have also found that the NGTVII's effective potential in the interior can be larger and deeper than that of the TVII model, indicating the deceleration of the echo time. Moreover, using the effective potential of NGTVII, the quasinormal mode and gravitational echo are calculated using Bohr-Sommerfeld fitting and solving the time-dependent Reggae-Wheeler equation. We can infer that the NGVTII with the maximum compactness and nonlocal parameter values enables the existence of the ultracompact star with more trapped modes.

DOI: 10.1103/PhysRevD.106.104020

I. INTRODUCTION

As a classic theory, general relativity (GR) passed almost all precision tests on broad energy scales. However, from a theoretical view GR faces two main problems. The first is the occurrence of singularity in cosmology and black hole (BH). Second, this theory is nonrenormalizable when we quantize with the standard method. Furthermore, the presence of singularities in BHs, not only in GR but also in most of the modified gravity theories formulated classically. A resolution of this issue most likely requires considering the quantum effects. However, the quantum field on the BH background breaks the unitarity property of quantum theory [1,2]. Note that the nonlocality of spacetime might resolve this problem (see Ref. [3,4] and the references therein). The basic argument of these inevitable procedures occurs because spacetime, in the Planck scale, slowly shifts its nature to the cutoff in the ultraviolet regime (short wavelength). Therefore, all of the extensive studies of quantum gravity, such as noncommutative geometry [5–20] and the generalized uncertainty principle [21–32] employ the idea of the fundamental length and seem nonlocal in the conventional sense. Moreover, most of the nonlocal gravity theory has already been studied in the physics of BHs [33–41]. Some of the references improved the solution by adding some corrections in the nonlocal action with an entire function, $\mathcal{A}(\Box)$. In [33] the author obtained the BH solution using a noncommutative black hole (NCBH) with the entire function of the order $1/2$ and generalized uncertainty principle (GUP) with the entire function of the order lower than $1/2$. Studies revealed that the BH with the nonlocal contribution enables the existence of static and vacuum BH with

(1) Regular properties at the center,
(2) Zero remnant value in the Hawking temperature,
(3) Positive heat capacity.

Therefore, we can infer that nonlocal gravity could be a good candidate for curing the conventional defect of classical gravity at the Planck scale.

Compact objects can be classified based on their compactness $C \equiv M/R$. For BHs $C = 1/2$. White dwarfs and neutron stars have compactness $C < 1/3$. The third set of compact objects are objects with compactness ranging between $4/9 < C < 1/2$. These exotic compact objects violate the Buchdahl limit. As denoted by ultracompact

[*]byon.nugraha91@ui.ac.id
[†]ilham.prasetyo@sci.ui.ac.id
[‡]anto.sulaksono@sci.ui.ac.id
[§]hramad@sci.ui.ac.id

stars in this work, are the fourth kind of compact object with a compactness ranging between $1/3 < C < 4/9$. These stars do not violate the Buchdahl limit but they possess a photon sphere; the photon sphere is the unstable circular null geodesic of the external Schwarzchild spacetime metric. Note that when objects have a photon sphere that manifested from a compact binary merger process, the postmerger ringdown waveform could be initially identical to the one of a BH with modifications encoded in subsequent pulses of gravitational wave known as gravitational echos [42]. Please see a review of the classification and the properties of compact objects in Ref. [4] and the references therein. Therefore, exploring nonlocality's effect on ultracompact stars is intriguing.

GR and its alternative theory have extensively studied the exact solution for the static fluid star. Despite the increasing total number of the exact solutions [43], only several subsets of them can be matched with the physical condition. Most of the solutions represent the pathologies from the mathematical point of view, or do not satisfy the causality and the energy condition. One well-known example of the exact solutions is the constant density star (CDS) and the TVII star. The CDS model allows the star to have an incompressible fluid with a nonzero density in the star's interior and the pressure, which drops from its center to zero at the boundary. Despite the straightforward metric, the infinite speed of sound makes the matter content inside the star superluminal. However, this solution provides a clear prophecy about the maximum possible compactness in the Buchdal limit [44] i.e., $\mathcal{C} \leq 4/9$ (Please see also the discussion related to bound in ultracompact objects in Ref. [45] and for the anisotropic version in Ref. [46].). TVII was proposed by Tolman [47] where he developed a general method to obtain the static spherically-symmetric Einstein equations with matter fluid sources. The purpose of this method is to obtain the gravitational equilibrium with a perfect fluids solution easily and open up several exact solution possibilities to explore the interior model of the star. This method accommodates eight exact solutions for the metric functions, matter density, and fluid pressure. Among the eight solutions, the first three are well known, i.e., The Einstein universe, The Schwarzschild-de Sitter solution, and the Schwarzschild interior, whereas the other four are somewhat unphysical. The TVII model is one of the interesting solutions of this kind because the model is physically quite acceptable [48–53]. TVII is an analytical model with a simple quadratic function on the density profile. The profile becomes zero at the surface and haas nonzero finite values in the center. The pressure profile also shows similar behavior. This model satisfies all energy conditions except the dominant energy condition (DEC). It has been reported that the TVII model has a maximum compactness, $\mathcal{C}_{\max} = 0.38$ and DEC can be satisfied up to photon sphere compactness i.e., $\mathcal{C}_{\rm ps} = 0.33$ [54,55]. Moreover, the sound of speed near the center, $c_s|_{r\to 0}$, in the TVII model allows the subluminal condition only for the compactness quite far below $\mathcal{C}_{\rm ps}$.

Gravitational perturbation of compact stars provides information on echo time, effective potential, quasinormal mode (QNM), and the gravitational echo signal. These quantities becomes crucial and relevant in the gravitational-wave era because they could experimentally be observed. The gravitational-wave modes due to perturbation can be classified into two distinct families, i.e., the axial and the polar modes. In this work, we focus only on the oscillation of the axial mode obtained by solving the Regge-Wheeler equation. For the TVII model, the axial mode has extensively been studied in Refs. [56–61]. It was shown that the compactness below $\mathcal{C}_{\rm ps}$ can still have a *w*-mode. The axial and polar modes as well as the QNM of neutron stars (NS) within the TVII model are explored in detail in Ref. [62]. On the other hand, it was shown in Ref. [63] for the static case and in Ref. [64] for the rotating case that the Tolman VIIs effective potential of NS obtained from the null geodesics with $R_{\min}/M = 2.59$ can trap gravitational waves or neutrinos. At the same time, there has been an extensive study on nonradial oscillations within the TVII model. The most exciting of the axial mode oscillations is the trapped mode. This mode does not have a Newtonian counterpart [65], and its mode increases when the star is already in the ultracompact region. Thus, related to the damping time, we can imply that the more compact the star is, the slower the damping is because the gravitational waves are trapped inside the effective potential barrier.

In this paper we investigate the impact of including nonlocality to the TVII model using the nonlocal form shown in Ref. [33]. There are many discussions on the impact of nonlocality on black hole properties. This work focuses on the impact of nonlocality in ultracompact objects based on a fluid ideal. It means that the interior of the corresponding ultracompact star equation of state is assumed to be perfect fluid. Therefore, the equation of state should satisfy the well-known energy conditions (strong energy condition, dominant energy condition, weak energy condition, and null energy condition). Therefore, the maximum compactness for a given equation of state is expected only to be less than the Buchdal limit value; $\mathcal{C}_{\rm BL} = 4/9$ [4]. So the condition with $\mathcal{C} > \mathcal{C}_{\rm BL}$ makes the pressure as well as the tensor metric infinite in this picture. In addition, TVII [52] is a perfect fluid, analytic model. This model is more realistic than constant density star model. However, the price we must pay is the existence of the constraint compactness, $\mathcal{C}_{\max} = 0.38$. So it is still intriguing to obtain the best model of the star to smear the TVII to be a good candidate and, perhaps, reach wider compactness until near the Buchdal limit value. The latter is the main motivation of this work. On the other hand, considerable attention has been devoted to studying the black hole mimicker objects [66–68]; one of this kind is a gravastar [69]. This object allows us to explore the

compactness higher than the Buchdal limit. However, the violation of the strong and dominant energy conditions can not be avoided in this model. Since our object still clings firmly to the perfect fluid assumption and does not exhibit the black hole mimicker objects, the novel solution is valid only in the range of the ultracompact region below the Buchdal limit.

We suspect that the nonlocality makes the star's compactness higher. Therefore, we could study the ultracompact stars within the TVII model. Consequently, the analysis of the echo time, QNM, and the gravitational echo in the ultracompact region become more viable to explore within this model. We note that embedding the nonlocal effect into a compact object has been an intriguing problem in astrophysics. Note that the ultracompact object with two potential barriers modeled by two Dirac delta potentials endowed in the nonlocal scalar field reveals that the echoes in that object can be amplified [70]. It was also shown in Ref. [71] that the quark and neutron stars within the nonlocal gravity (with positive coefficient) enable the existence of the highest maximum mass compared to GR limit counterpart. Please see also Refs. [72–76] for detailed discussion of the nonlocal impacts on the stars.

This paper is structured as follows: In Sec. II we briefly review the TVII model. In Sec. III we discuss nonlocal gravity impacts in the TVIII model, the analytic density, and the numerical profile of the pressure, and the metric $e^{\nu(r)}$. Before we discuss the perturbation of the star and the related properties, we check the validity of the solution and the parameters presented in Sec. IV; the physically allowed nonlocal parameter $\tilde{\beta}$ and the compactness $\mathcal{C}$ are discussed. Section V provides calculation results for gravitational perturbation in the axial case. Hence, QNM and the gravitational echo are discussed. In Sec. VI, we conclude the discussion. We also present some calculations detailed in the Appendix. We use the geometrized units throughout the paper.

II. TOLMAN VII MODEL

To begin with, we will briefly review the TVII model. The metric used to describe nonrotating and spherically-symmetric objects is [47,52,53]

$$ds^2 = -e^{\nu(r)}dt^2 + e^{\lambda(r)}dr^2 + r^2 d\Omega^2, \tag{1}$$

where the tt and rr components are a function of r, and $d\Omega^2 = d\theta^2 + \sin^2\theta d\varphi^2$ is a two-sphere element. The matter in the interior of the object within ideal fluid approximation takes following form

$$T_{\mu\nu} = (\rho + p)u_\mu u_\nu + p g_{\mu\nu}, \tag{2}$$

where ρ and p are the energy density and the pressure, respectively, whereas u_μ is the four-velocity. From the Einstein field equation, $G_{\mu\nu} = 8\pi T_{\mu\nu}$, we can have the following equations

$$m' = 4\pi r^2 \rho, \tag{3}$$

$$e^{-\lambda}\left(\frac{\nu'}{r} + \frac{1}{r^2}\right) = 8\pi p, \tag{4}$$

$$\left(\frac{e^{-\lambda}-1}{r^2}\right)' + \left(\frac{e^{-\lambda}\nu'}{2r}\right)' + e^{-(\lambda+\nu)}\left(\frac{e^{\nu}\nu'}{2r}\right)' = 0. \tag{5}$$

Note that the prime symbol $'$ denotes d/dr and $e^{-\lambda} \equiv 1 - 2m(r)/r$. In the Tolman VII model, the corresponding energy density profile is defined in a simple quadratic form which can be written as

$$\rho(r) \equiv \rho_c[1 - (r/R)^2], \tag{6}$$

where ρ_c is the energy density value at the object's center and R is a stellar radius. From these equations, we can obtain a complete solution of the metric inside the star within the TVII model. Putting the density profile into Eq. (3) and integrating it with the appropriate choices of boundary conditions in $r = R$ gives us the mass profile of this model as

$$m_{\mathrm{TVII}}(r) = 4\pi\rho_c\left(\frac{r^3}{3} - \frac{r^5}{5R^2}\right), \tag{7}$$

and hence, the explicit value of ρ_c can be obtained by using the condition that $M \equiv m(R)$. The result is $\rho_c = 15M/8\pi R^3$. Then, we can obtain the metric in the rr component as

$$e^{-\lambda_{\mathrm{TVII}}}(r) = 1 - \frac{8\pi}{15}\rho_c r^2\left(5 - \frac{3r^2}{R^2}\right). \tag{8}$$

This result can be used to get the ν function by substituting the latter equation into Eq. (5). The result reads

$$e^{\nu_{\mathrm{TVII}}}(r) = C_{1,\mathrm{TVII}}\cos^2[\phi_{\mathrm{TVII}}(r)], \tag{9}$$

where

$$\phi_{\mathrm{TVII}}(r) = C_{2,\mathrm{TVII}} - \frac{1}{2}\log\left|\frac{r^2}{R^2} - \frac{5}{6} + \sqrt{\frac{5e^{-\lambda_{\mathrm{TVII}}}}{8\pi\rho_c R^2}}\right|. \tag{10}$$

The $C_{1,\mathrm{TVII}}$ and $C_{2,\mathrm{TVII}}$ are defined as

$$C_{1,\mathrm{TVII}} \equiv 1 - \frac{5\mathcal{C}}{3}, \tag{11}$$

$$C_{2,\mathrm{TVII}} \equiv \tan^{-1}\left[\sqrt{\frac{\mathcal{C}}{3(1-2\mathcal{C})}}\right] + \frac{1}{2}\log\left|\frac{1}{6} + \sqrt{\frac{1-2\mathcal{C}}{3\mathcal{C}}}\right|, \tag{12}$$

where the compactness $\mathcal{C} \equiv M/R$. These integration constants are determined from the boundary condition in $r = R$; by matching the exterior solution with the zero pressure value at the object's surface. As we mentioned earlier, the allowed maximum compactness (based on the finiteness of the pressure and the metric) for the TVII model is restricted until $\mathcal{C}_{\max} \approx 0.38$ [54].

III. NONLOCAL GRAVITY WITH TOLMAN VII (NGTVII) MODEL

In this section we construct TVII under nonlocal gravity. The nonlocality in the gravity sector can be mapped into the nonlocality in the matter sector. In this work, we use the action proposed in Ref. [33]. This nonlocality model has been used recently to study the impact of nonlocality in a black hole (BH) [34–37]. The action is [33]

$$S = \frac{1}{16\pi}\int d^4x\sqrt{-g}\mathcal{R}(x) + S_{\text{matter}}, \tag{13}$$

where the ordinary Ricci tensor, R, is embedded through the following form

$$\mathcal{R}(x) = \int d^4y\sqrt{-g}\mathcal{A}^2(x-y)R(y), \tag{14}$$

and the bilocal distribution is defined by

$$\mathcal{A}^2(x-y) \equiv \mathcal{A}^2(\Box_x)\delta^{(4)}(x-y). \tag{15}$$

Here, the operator $\mathcal{A}(\Box_x) = g_{\mu\nu}\nabla^\mu\nabla^\nu$, is dimensionless d'Alembertian operator. We can obtained the Einstein field equation (EFE) by varying the action in Eq. (13) with respect to the metric tensor $g_{\mu\nu}$ and neglecting the surface term related to the variation of the d'Alembertian. The nonlocal EFE reads

$$\mathcal{A}^2(\Box)\left(R_{\mu\nu} - \frac{1}{2}g_{\mu\nu}R\right) = 8\pi T_{\mu\nu}. \tag{16}$$

The bi-local operator works on the gravity sector. However, the EFE can be written in the following form

$$R_{\mu\nu} - \frac{1}{2}g_{\mu\nu}R = 8\pi\mathcal{T}_{\mu\nu}, \tag{17}$$

where $\mathcal{T}_{\mu\nu} \equiv \mathcal{A}^{-2}(\Box)T_{\mu\nu}$. It is allowed since $\mathcal{A}$ has a unique and well-defined inverse [33]. Now, the action (13) can be represented in two possible ways; Eq. (16) denotes the nonlocal geometry coupled to the ordinary matter, whereas Eq. (17) denotes the ordinary local gravity coupled to the generalized matter. The two forms are equivalent [33]. In the entire calculation in this paper, we use Eq. (17) as the representation of nonlocal EFE to be solved because this option is easier to handle. The nonlocal effect appears in the matter sector, and hence, the tensor energy-momentum presented in Eq. (2) is modified into

$$\mathcal{T}_{\mu\nu} = (\tilde{\rho} + \tilde{p})u_\mu u_\nu + \tilde{p}g_{\mu\nu}, \tag{18}$$

and the three component of $G_{\mu\nu} = 8\pi\mathcal{T}_{\mu\nu}$ together with the r component from the continuity equation and ansatz (1) yield

$$e^{-\lambda}\left(\frac{\lambda'}{r} - \frac{1}{r}\right) + \frac{1}{r^2} = 8\pi\tilde{\rho}, \tag{19}$$

$$e^{-\lambda}\left(\frac{1}{r^2} + \frac{\nu'}{r}\right) - \frac{1}{r^2} = 8\pi\tilde{p}, \tag{20}$$

$$\frac{e^{-\lambda}}{4}\left(2\nu'' + \nu'^2 - \nu'\lambda' + \frac{2\nu'}{r} - \frac{2\lambda'}{r}\right) = 8\pi\tilde{p}, \tag{21}$$

$$\tilde{p}' = -\frac{1}{2}(\tilde{p} + \tilde{\rho})\nu'. \tag{22}$$

This EFE for the isotropic perfect fluid leads us to three ordinary differential equations for the matter variables, $\tilde{\rho}$ and $\tilde{p}$, and the two metric variables, ν and λ. These relations give us the Tolman-Oppenheimer-Volkof (TOV) equation as shown in Eq. (22). To evaluate it step by step, we employ the r component of the metric tensor to give a simple expression for mass when the generalized density, $\tilde{\rho}$, are known. Next, following the Tolman idea to manipulate the components of the EFE in Eqs. (20) and (21), the set of field equations reduces to second-order differential equation for metric ν, which already appeared in Eq. (5). Next, with the aid of $e^{-\lambda}$, Eq. (19) turns out into

$$m' = 4\pi r^2\tilde{\rho}. \tag{23}$$

Our next task is to obtain the modified nonlocal density profile. We start with the definition of the density itself as

$$\tilde{\rho} = \mathcal{A}^{-2}(\Box)\rho = \frac{1}{(2\pi)^3}\int_0^\infty ds e^{-s(1+\beta p^2)}\int d^3p\rho(p)e^{i\vec{x}.\vec{p}}, \tag{24}$$

$$\tilde{\rho} = \frac{1}{2\sqrt{\beta}x}\left[\int_0^x dx'x'\rho(x')e^{-\frac{x}{\sqrt{\beta}}}\left(e^{\frac{x'}{\sqrt{\beta}}} - e^{-\frac{x'}{\sqrt{\beta}}}\right) + \int_x^R dx'x'\rho(x')e^{-\frac{x'}{\sqrt{\beta}}}\left(e^{\frac{x}{\sqrt{\beta}}} - e^{-\frac{x}{\sqrt{\beta}}}\right)\right]. \tag{25}$$

After some algebra, we finally obtain the close form expression for the modified nonlocal density. The calculation detail can be seen in the Appendix. While in general we can put this modified nonlocal density into any model, in this work we use it only for the case of the TVII model. Changing variables and inserting the model into Eq. (25) gives

$$\tilde{\rho}(r) = \tilde{\rho}_c e^{-\frac{r+R}{\sqrt{\beta}}}\left[\left(\frac{\sqrt{\beta}}{r}+\frac{3\beta}{rR}+\frac{3\beta^{\frac{3}{2}}}{rR^2}\right)(e^{\frac{2r}{\sqrt{\beta}}}-1)-e^{\frac{r+R}{\sqrt{\beta}}}\left(\frac{r^2}{R^2}+\frac{6\beta}{R^2}-1\right)\right]. \tag{26}$$

The modified nonlocal density profile is characterized by its stellar radius R, nonlocal parameter β as well as the energy density value at the center. In order to get the expression for ρ_c, we demand the same condition as used in the standard TVII model, and the result reads

$$\tilde{\rho}_c = \frac{15\mathcal{C}R^3\beta^{-5/2}e^{\frac{2R}{\sqrt{\beta}}}}{60\pi\left(\frac{R}{\sqrt{\beta}}+1\right)\left(3+\frac{R^2}{\beta}+\frac{3R}{\sqrt{\beta}}\right)+4\pi e^{\frac{2R}{\sqrt{\beta}}}\left(-45+\frac{2R^5}{\beta^{5/2}}-\frac{15R^3}{\beta^{3/2}}+\frac{30R^2}{\beta}\right)}. \tag{27}$$

As expected, the $\tilde{\rho}_c$ form is constituted from the compactness, stellar radius, and the nonlocal parameter. When β is small, the energy density profile and its value in the center are smoothly transformed into the ordinary ones. After this step, the mass profile $m(r)$ could be obtained by integrating Eq. (3). Note that based on the physical consideration, we also demand that the mass function must vanish at the core. To this end, we obtain the mass profile as

$$m_{\mathrm{NGTVII}}(r) = \frac{4\pi e^{-\frac{r+R}{\beta}}\tilde{\rho}_c\beta^{5/2}}{15R^2}\left\{15\left(3+\frac{R^2}{\beta}+\frac{3R}{\sqrt{\beta}}\right)\left[e^{2r/\sqrt{\beta}}\left(\frac{r}{\sqrt{\beta}}-1\right)+\frac{r}{\sqrt{\beta}}+1\right]-\frac{r^3e^{\frac{r+R}{\sqrt{\beta}}}}{\beta^{3/2}}\left(30+\frac{3r^2}{\beta}-\frac{5R^2}{\beta}\right)\right\}, \tag{28}$$

Furthermore, with the nonlocal mass and the density profiles in hand, we are ready to solve the second-order differential equation for metric ν. When we discussed TVII model, all the solutions we obtained were straightforward or analytical. Different cases appear when we consider a nonlocal effect where the solution for Eq. (5) cannot solve it analytically anymore. Hence, we try to solve those equations, i.e., Eqs. (5) and (22) numerically using *Mathematica* package. The solution for g_{tt} as well as the pressure depends on how we treat the nonlocal parameter β and the compactness $\mathcal{C}$. In the next section we will present the range of allowed values of parameter $(\beta, \mathcal{C})$ and also depict the plot related to the allowed parameter.

IV. IMPACTS OF NONLOCALITY ON THE EQUATION OF STATE PREDICTED BY TVII MODEL

In this section we discuss the numerical solution compared with the ordinary TVII model in detail. As explained earlier, the nonlocal contribution makes the differential equation no longer analytic. Hence, we must employ the suitable value for the compactness and the nonlocal parameter, respectively. In TVII model, the maximum compactness is $\mathcal{C}_{\max} = 0.38$. On the other hand, the NGTVII model has a nonlocal parameter in Eq. (5). Therefore, we could play with those parameters to obtain a relatively larger maximum compactness, $\mathcal{C}_{\max}$. The detailed numerical step and result will be presented below.

A. Allowed parameter and the causal condition

The second order differential equation presented in Eq. (5) can be solved numerically by setting

$$\nu = \nu_1, \qquad \nu' = \nu_2, \quad \text{and} \quad \nu'' = \nu_2'. \tag{29}$$

Substituting these definitions into Eq. (5) and followed by inserting the value of β and $\mathcal{C}$ with suitable boundary conditions that fit the exterior solution, we obtained the metric function $\nu(r)$ in a numerical data form. Next we substitute the $\nu(r)$ function into the TOV equation (22) to obtain the nonlocal pressure profile. However, in general, we already have a complete metric solution with the density and the pressure, describing NGTVII. Since the nonlocal parameter and the compactness mainly characterize the solution, we investigate the allowed parameter to have an existing solution for NGTVII's star. Besides, the causality condition is crucial for a physically acceptable star since, according to the initial observer, the cause and its consequence are separated in the timelike region. Hence, the object with a higher light speed violates the causality principle. The causal condition in the isotropic generalized perfect fluid can be compactly expressed as

$$0 \le c_s \le 1, \tag{30}$$

where $c_s \equiv \sqrt{d\tilde{p}/d\tilde{\rho}}$. This condition implies that the speed of sound, the c_s profile, must be positive and lay in the subluminal range of Eq. (30), for otherwise c_s becomes superluminal. A typical trend of the speed of sound as a function of r of certain gravitation objects is similar to the pressure profile, i.e., drops at the near-surface and reaches the maximum in the center. Hence we only focus on the region near the center, $c_{sr\to 0}$, and varied numerically with the compactness and the nonlocal parameter $\tilde{\beta}$. Note that $\tilde{\beta} \equiv \beta/10^2$.

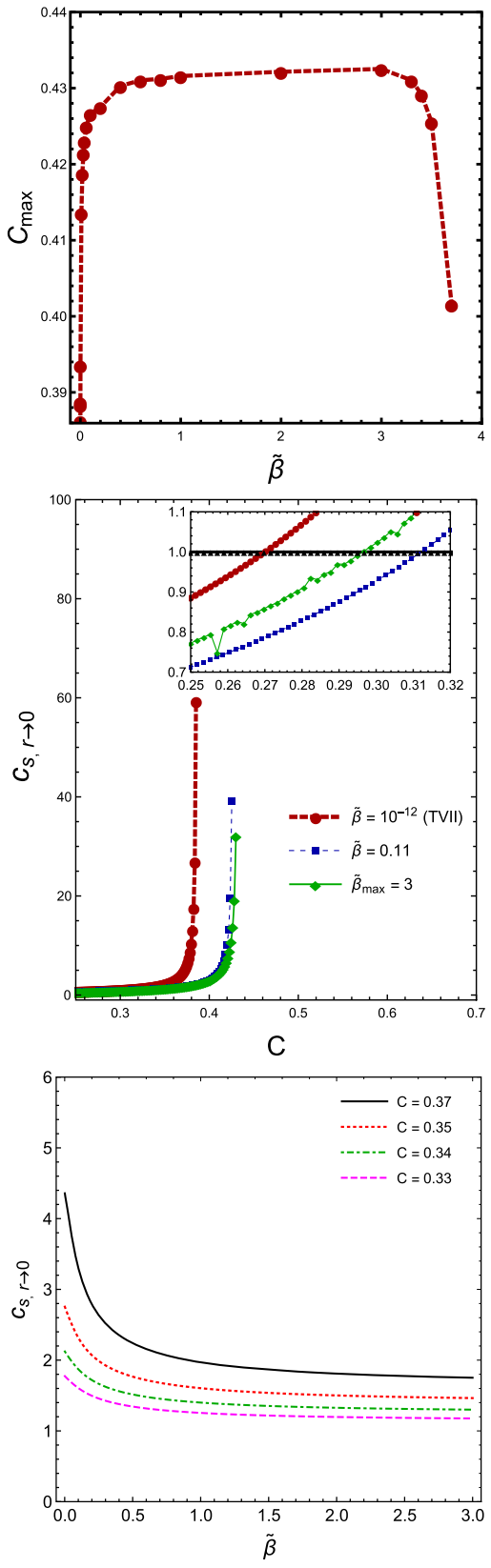

FIG. 1. [Top panel] Compactness maximum $\mathcal{C}_{\max}$ as a function of nonlocal parameter $\tilde{\beta}$. [Middle panel] Speed of sound near center as a function of compactness. [Bottom panel] and nonlocal parameter, respectively. Note that $\tilde{\beta} \equiv \beta/10^2$.

The allowed parameter and the causal condition are depicted in Fig. 1. On its top panel we plot the relationship between the compactness and the nonlocal parameter. Standard TVII model compactness can be obtained by setting the nonlocal parameter $\tilde{\beta}$ close to zero. However, for $\tilde{\beta} = 10^{-12}$ the result is already identical with $\tilde{\beta} \equiv 0$. It can be observed from this figure that when we shift β into a higher value, the compactness increases. Therefore, we could infer that the nonlocality of the matter sector enables the existence of a more compact star than that predicted by its TVII model counterpart. Thus, we focus on the $\tilde{\beta}_{\max} = 3$ with the maximum compactness $\mathcal{C}_{\max} = 0.43$. On the other hand, the middle and the bottom panels in Fig. 1 represent the speed of sound as a function of compactness with fixed nonlocal parameter $\tilde{\beta}$ and a function of $\tilde{\beta}$ with fixed compactness, respectively. The middle panel shows that for compactness value near the $C_{\rm ps}$, the ultracompact stars within NGTVII model can admit the causal condition $(c_s < 1)$ only for a certain small $\tilde{\beta}$ values. For example, this condition is satisfy for the case of $\tilde{\beta} = 0.11$. It is reported [54] that the speed of sound near the center for TVII admits the causal condition when[1] $\mathcal{C} \lesssim 0.26$. Thus, comparing our result we can infer that the nonlocal effect for a small value of $\tilde{\beta}$ enables the existence of an equation of state (EOS) that satisfies the subluminal condition in higher compactness than that of the local TVII model. In the bottom panel, we plot the speed of sound near the center as a function of $\tilde{\beta}$ with different compactness. it is evident that c_s, tends to have near-constant value when the nonlocal parameter, $\tilde{\beta}$, were shifted to higher value. When $\mathcal{C} = 0.37$, the star also tends to have a superluminal condition in all $\tilde{\beta}$ values. From this benchmark, it is without doubt that the ultracompact star with $\mathcal{C}_{\max}$ and $\tilde{\beta}_{\max}$ in the NGTVII model also cannot satisfy the causal condition. Despite the limitation, we can infer that the nonlocal effect allows the ultracompact stars to satisfy the sub-luminal conditions with compactness close to $C_{\rm ps}$, which is higher than that of Tolman VII counterpart [54].

From these considerations, we extract two values in order to analyze other properties of the NGTVII, including the effective potential, quasinormal mode and the gravitational echo. The maximum, $\mathcal{C}_{\max} = 0.43$ with $\tilde{\beta}_{\max} = 3$ as well as the parameter admiting the physical condition, $\mathcal{C} = 0.31$ with $\tilde{\beta} = 0.11$. The results are compared to that of TVII with $\mathcal{C}_{\max} = 0.38$.

B. Energy condition

The physically acceptable density profile and the pressure should satisfy the energy conditions. Therefore, it is crucial to check whether the equation of state of ultracompact stars within the NGTVII model satisfies the

[1]This information can be found in the Figs. [7–8] in [54].

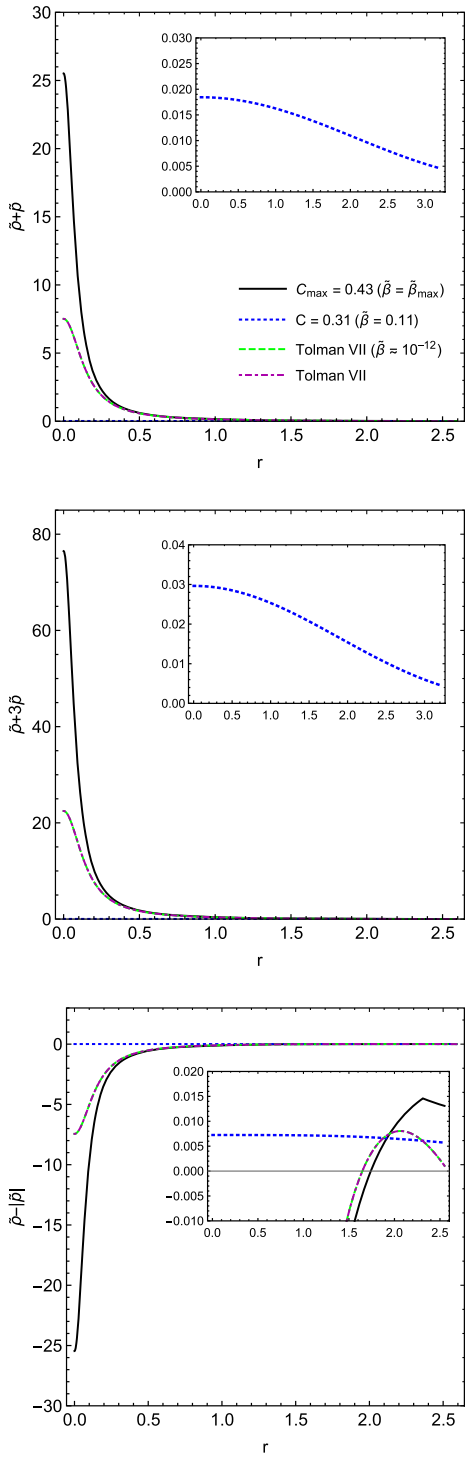

FIG. 2. The top, middle, and bottom figures represent the pressure and density combination profiles related to energy conditions for some parameter variations. The black solid line represents the density and the nonlocal pressure when $\tilde{\beta}_{\max}$ with $\mathcal{C}_{\max} = 0.43$. The blue dashed line represents the appropriate choices of $\mathcal{C}$ and $\tilde{\beta}$ that fit with the physical condition ($c_s < 1$). The green and magenta (dashed and dot-dashed) lines denote the one of TVII model with $\tilde{\beta} = 10^{-12}$ with $\mathcal{C}_{\max} = 0.38$.

energy condition or not. The energy conditions can be categorized into four types, i.e., strong energy condition (SEC), weak energy condition (WEC), dominant energy condition (DEC), and null energy condition (NEC). These conditions can be expressed mathematically as

$$\text{SEC}: \tilde{\rho} + \tilde{p} \geq 0, \qquad \tilde{\rho} + 3\tilde{p} \geq 0, \tag{31}$$

$$\text{DEC}: \tilde{\rho} \geq |\tilde{p}|, \tag{32}$$

$$\text{WEC}: \tilde{\rho} \geq 0, \qquad \tilde{\rho} + \tilde{p} \geq 0, \tag{33}$$

$$\text{NEC}: \tilde{\rho} + \tilde{p} \geq 0. \tag{34}$$

This paper also assumes that the matter's nonlocal pressure is isotropic. From these equations, the SEC denotes the strong repulsion of gravity, and the summation of the nonlocal density and the nonlocal pressure should be positive. The DEC denotes that the nonlocal density should be higher than the nonlocal pressure. The WEC and NEC are relatively similar. However, the WEC needs additional requirements that the nonlocal density should be positive also.

We present the pressure and density combination profiles in the top, middle, and bottom panels of Fig. 3 for the parameter variations shown in the figures. The trend of shapes of the profiles in the top and middle panels are pressurelike profiles. The NEC and WEC are satisfied by the models' equation of state. Since we have a positive value for the density and the pressure. The SEC is also satisfied because $\tilde{\rho} + 3\tilde{p}$ is greater than $\tilde{\rho} + \tilde{p}$. The DEC presented in the bottom panel means that the subtraction between density and the absolute pressure must be positive. In the figure it is evident that the differences become negative in the near the center region (black line and the TVII model). This evidence indicates the violation of the DEC in this region.

In the TVII model, the $\rho - |p|$ profile drops moderately to zero at the surface, whereas, in the NGTVII, the profile drops to some finite value. It happens because they have different density profiles. We have found that the nonlocality effect in NGTVIII cannot be fully remedied, but this issue can be reduced if the compactness is less than the maximum compactness value. According to the causal condition, compactness near the photon sphere with small $\tilde{\beta}$ admits the causal condition and is depicted as a blue dashed line in Fig. 2. The $\tilde{\rho} - |\tilde{p}|$ is positive at all interior regions of the NGTVII's star. Thus, the DEC is fully fulfilled and higher than TVII counterpart [55].

C. Solution

We calculate the density of TVII and NGTVII models analytically. The results are depicted in the top panel of Fig. 3 with the parameter variations shown in the box. The

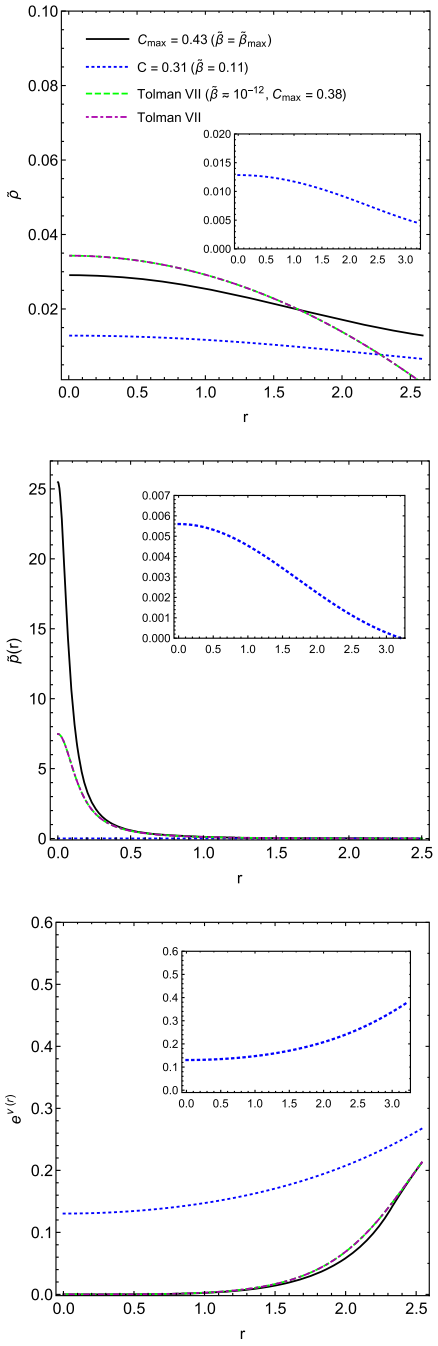

FIG. 3. [Top panel] Generalized energy density as a function of stellar radius. [Middle panel] Nonlocal pressure profile as a function of r. [Bottom panel] $e^{2\nu}$ metric profile as a function of r. The black line represent maximum parameter, $\tilde{\beta}_{\max} = 3$ with $\mathcal{C}_{\max} = 0.43$. The blue dashed line denotes the physical condition ($c_s < 1$) with $\mathcal{C} = 0.31$ and $\tilde{\beta} = 0.11$. The green dashed line denotes the TVII model with $\tilde{\beta} = 10^{-12}$ and $\mathcal{C}_{\max} = 0.38$, and the magenta dotted-dashed line represents the TVII model solution. In this figure, we can show that the small nonlocal parameter and the pure TVII model always coincide.

black line represents the maximum parameter that NGTVII have, $\tilde{\beta}_{\max} = 3$ with $\mathcal{C}_{\max} = 0.43$. The blue dashed line denotes the parameter that fits with the physical condition ($c_s < 1$) with $\mathcal{C} = 0.31$ and $\tilde{\beta} = 0.11$. The green dashed line denotes the TVII model with $\tilde{\beta} = 10^{-12}$ and $\mathcal{C}_{\max} = 0.38$, and the magenta dotted-dashed line represents the TVII model solution. For the TVII model, the ultracompact equation of motion tends to have a finite value density at the center and smoothly drop to zero at the star's surface. The inclusion of nonlocality in the model modifies the surface properties of the stars. The density profile of NGTVII has a finite density value at the surface. We also ensure that our result reduces to the well-known TVII model result when we limit the $\tilde{\beta}$ closer to zero.

We also have plotted the nonlocal pressure to r in the middle panel of Fig. 3. We have found that the general trend of the corresponding pressure profiles is physically proper up to certain maximal values of β and $\mathcal{C}$. However, for particular values of β and compactness $\mathcal{C}$ larger than the corresponding maximum values, the $\nu(r)$ and $\tilde{p}$ profiles become infinite near the center. Therefore, the pressure profiles become unphysical in this region. The plots in the middle panel of Fig. 3 are the same at the near surface since we employ the same boundary condition $\tilde{p}(R) = 0$. However, if we move to the region closer to the center, we have center pressure $\tilde{p}_c$. It is also shown from the figure that the p_c abruptly increases, and it becomes larger than the one of TVII when the compactness increases until it is closer to maximum compactness (with $\tilde{\beta}_{\max}$). In the bottom panel, the metric e^{ν} profile is plotted in Fig. 3 and calculated with different compactness and nonlocality parameter values. The black line (NGTVII) and the green/magenta line (TVII) coincide from near the center, and they split as the radius becomes large. The metric of the NGTVII model, which admits the physical condition (blue dashed line), yields a larger metric value than that of the TVII model.

To this end, we have systematically explored the equation of state predicted by the NGTVII model numerically with the appropriate boundary condition. We can infer that the range of the compactness can increase until $\mathcal{C}_{\max} = 0.43$ with $\tilde{\beta}_{\max} = 3$. Up to these parameter values, we investigated the modified nonlocal density, pressure, energy condition, and speed of sound and compared them to those of the TVII model. We have found that the ultracompact star within these models ($\mathcal{C}_{\max}$ and $\tilde{\beta}_{\max}$) does not satisfy the causal condition. Note that this violation also appears in the well-known constant density star and Tolman VII model. The CDS has an incompressible energy density. However, the nonlocality of NGTVII model allows us admit the causal condition and the DEC when the nonlocal parameter is small with the compactness near $\mathcal{C}_{\text{ps}}$.

V. PERTURBATION OF THE STARS

It is well known that the production of the gravitational wave echo due to the ringdown of the photon sphere's unstable orbit could be observed for the ultracompact objects with compactness between $0.33 \leq \mathcal{C} \leq 0.44$. The TVII model is valuable for describing ultracompact objects since the TVII model has an analytic energy density that is finite in the center and has zero value at the surface. However, we need to note that several authors reported that the validity of the TVII model to describe the ultracompact objects is restricted only until $C_{\max} \approx 0.38$ because it has divergent pressure and g_{tt} metric in this limit. This limit is still larger than the photon sphere limit, i.e., $C_{\rm ps} = 0.33$. In the previous section we presented the Einstein field equation and the numerical method to calculate the properties of ultracompact stars within the NGTVII model. With some choices of nonlocal parameters, we can shift the compactness cutoff to larger than the TVII model. Here, we discuss the QNM and gravitational echo of ultracompact objects within the NGTVII model. First, we construct the gravitational waves by employing the perturbation into the Einstein field equation of the NGTVII model using the general ansatz for perturbation proposed by Chandrasekar [77] to obtain the wave equation. After that, we discuss the effective potential, the corresponding implications on QNM, and the gravitational echo.

A. Regge-Wheeler equation and effective potential

It can be shown that we can obtain (from Einstein's field equations) the several forms of nonzero Ricci tensors from a perturbed metric that can be evaluated and expressed them as following differential equations [77]

$$\begin{aligned}
&(e^{3\psi-\nu-\mu_2-\mu_3}Q_{23})_{,\theta} + e^{3\psi-\nu-\mu_2+\mu_3}Q_{02,0} = 0,\\
&(e^{3\psi-\nu-\mu_2-\mu_3}Q_{23})_{,r} - e^{3\psi-\nu+\mu_2-\mu_3}Q_{03,0} = 0,\\
&\text{where } Q_{AB} = q_{A,B} - q_{B,A} \quad \text{and} \quad Q_{A0} = q_{A,0} - \omega_{,A}\ (2,3).
\end{aligned} \tag{35}$$

With the aid of these two latter equations, we can obtain

$$\begin{aligned}
&[e^{-3\psi+\nu+\mu_2-\mu_3}(e^{3\psi+\nu-\mu_2-\mu_3}Q_{23})_{,3}]_{,3}\\
&\quad + [e^{-3\psi+\nu+\mu_2+\mu_3}(e^{3\psi+\nu-\mu_2-\mu_3}Q_{23})_{,2}]_{,2} = Q_{23,0,0}.
\end{aligned} \tag{36}$$

Equation (36) can be separated by expanding the function in terms of Gegenbauer function $\mathcal{C}_n^{\alpha}(\theta)$, that satisfiying following differential equation

$$\left[\frac{d}{d\theta}\sin^{2\alpha}\theta\frac{d}{d\theta} + n(n+2\alpha)\sin^{2\alpha}\theta\right]\mathcal{C}_n^{\alpha}(\theta) = 0. \tag{37}$$

Using the separable equation defined as

$$\begin{aligned}
&e^{3\psi+\nu-\mu_2-\mu_3}Q_{23} = r\Psi(r)\mathcal{C}_{l+2}^{-3/2}(\theta),\\
&\text{and introducing } \frac{dr_*}{dr} = e^{-\nu+\mu_2},
\end{aligned} \tag{38}$$

the tortoise radial coordinate, Eq. (36) can be reduced to the time-dependent wave equation in r_* as

$$\left[\frac{\partial^2}{\partial t^2} - \frac{\partial^2}{\partial r_*^2} + V(r)\right]\Psi(r_*, t) = 0, \tag{39}$$

where the effective radial potential is

$$V(r) = \frac{e^{\nu}}{r^3}[l(l+1)r + 4\pi r^3(\tilde{\rho} - \tilde{p}) - 6\tilde{m}(r)]. \tag{40}$$

Note that we obtain the Regge-Wheeler equation with the pressure, density, and mass defined in a nonlocal manner. The second-order partial differential equation described above was endowed with three essential physical ingredients, i.e., the effective potential, complex eigenvalue, and the time-dependence eigenfunction. Therefore, first, we want to analyze the effective potential behavior. Inside the star, we use the effective interior potential, whereas outside the star, we use the exterior. In Fig. 4 we show the effective potential as the function of the radius. The detailed information about the plots is explained in the figure caption of Fig. 4. Here, we consider TVII and NGTVII models to be in the compactness range of ultracompact objects i.e., $0.33 \leq \mathcal{C} \leq 0.44$. The star's surface is located at $R < 3M$, and the exterior solution has a barrier at $R \approx 3M$. This is where the unstable circular null geodesics or light ring occurs. A perturbed star's effective potential enables the infinite potential value to exist at the center since the presence of the centrifugal contribution. From the figure we can infer that the effective potential of the ultracompact star allows the presence of the well between the light ring and the center. The TVII and NGTVII effective potentials also possess a second light ring at the minimum of the effective potential. Since it has a positive value of the second derivative of the potential, the second light ring should be stable. It can be reported that the nonlocal contribution with $\mathcal{C}_{\max}$ makes the interior potential deeper than the TVII's potential. When we shift the attention to the blue dashed line, it exhibits a tiny well in the star's interior. Hence, this parameter makes the quasinormal mode hard to excite, and the axial modes are not resonant. The bottom panel's effective potential with the higher l increases the barrier.

However, it is convenient to discuss the effective potential of the tortoise coordinate. The relation between the coordinate and the radius is

$$r_* = \int_0^r \sqrt{-\frac{g_{rr}}{g_{tt}}}dr, \tag{41}$$

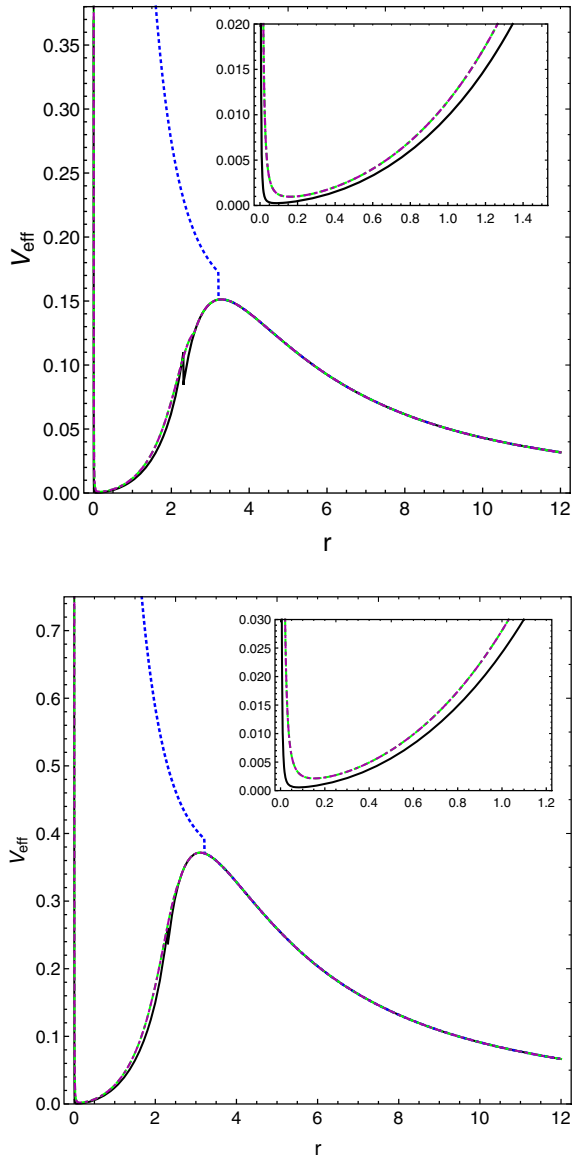

FIG. 4. V_{eff} as a function of r with $l = 2$ [Top panel] and $l = 3$ [Bottom panel]. The black line represent maximum parameter, $\tilde{\beta}_{\text{max}} = 3$ with $\mathcal{C}_{\text{max}} = 0.43$. The blue dashed line denotes the physical condition ($c_s < 1$) with $\mathcal{C} = 0.31$ and $\tilde{\beta} = 0.11$. The green dashed line denotes the TVII model with $\tilde{\beta} = 10^{-12}$ and $\mathcal{C}_{\text{max}} = 0.38$, and the magenta dotted-dashed line represents the TVII model solution.

where g_{tt} and g_{rr} are the metrics in the interior and the exterior region of the star. Evaluating Eq. (41) numerically, using the appropriate boundary condition, and matching with the exterior tortoise coordinate, we obtain the plots shown in Fig. 5. Figure 5 represents the relation betweem r_* and r for the cases $\mathcal{C}_{\text{max}} = 0.43$ with $\tilde{\beta}_{\text{max}} = 3, \mathcal{C} = 0.31$, with $\tilde{\beta} = 0.11$, and TVII parameter. We can also see that the value of the $r_*(0)$ are finite and becomes higher when compactness decrease. Furthermore, exterior region exhibit the linear relation between r_* and r.

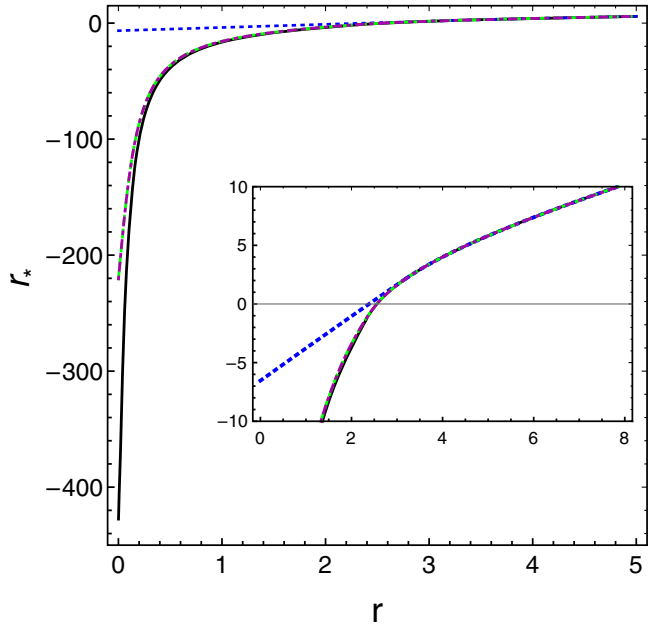

FIG. 5. r_* as a function of r. The black line represent maximum parameter, $\tilde{\beta}_{\text{max}} = 3$ with $\mathcal{C}_{\text{max}} = 0.43$. The blue dashed line denotes the physical condition ($c_s < 1$) with $\mathcal{C} = 0.31$ and $\tilde{\beta} = 0.11$. The green dashed line denotes the TVII model with $\tilde{\beta} = 10^{-12}$ and $\mathcal{C}_{\text{max}} = 0.38$, and the magenta dotted-dashed line represents the TVII model solution.

With r_* as a function of r in hand, we can obtain the effective potential as a function of r_* plots. Figure 6 shows both interior and exterior region of effective potential as a function of r_*. One can see that the compactness gives us information on how wide the interior potential in this figure is, whereas by comparing the top and bottom panels, it can be seen that the angular momentum l determines the height of the potential barrier. The nonlocal EOS of NGTVII with $\mathcal{C}_{\text{max}}$ provides a wider and deeper potential than the TVII potential. For the compactness admitting the causal condition, the potential well rapidly disappears and does not have a sufficient size of the well to produce a quasinormal mode and gravitational echoes. We can also infer that all horizonless ultracompact objects obtained in this work satisfied the null energy condition. They possess an unstable light ring. They also have a stable light ring [78]. These signatures are important for the production of gravitational echoes. In detail, the well of the potential is related to echo time. The deeper the well, the longer it will take for the echo to propagate through the interior of the ultracompact star. When the value of the β parameter is close to zero, the effective potential reduces to the well-known TVII model. Moreover, the earlier studies [79,80] revealed that the spectrum mode related to the potential could contain three kinds of spacetime modes, i.e., the trapped modes [81] that corresponds to the potential well predicted by ultracompact stars, and the w modes [82] that corresponds to the scattering on the top of the barrier, and

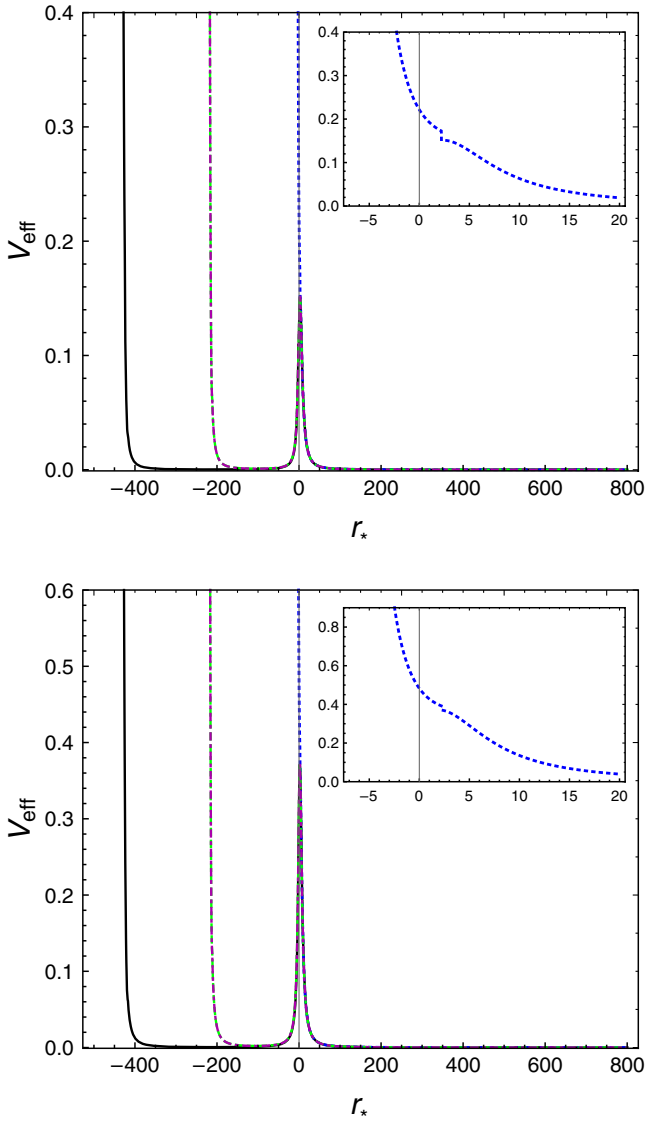

FIG. 6. $V_{\rm eff}$ as a function of r_* for $l = 2$ [Top panel] and $l = 3$ [Bottom panel]. The black line represent maximum parameter, $\tilde{\beta}_{\rm max} = 3$ with $\mathcal{C}_{\rm max} = 0.43$. The blue dashed line denotes the physical condition ($c_s < 1$) with $\mathcal{C} = 0.31$ and $\tilde{\beta} = 0.11$. The green dashed line denotes the TVII model with $\tilde{\beta} = 10^{-12}$ and $\mathcal{C}_{\rm max} = 0.38$, and the magenta dotted-dashed line represents the TVII model solution.

the w_{II} mode [83] that corresponds to the extremely fast damped mode. In the next subsection we discuss only the mode crucial for ultracompact stars (axial part), i.e., the trapped mode.

B. Echo time and quasinormal mode

Echo time defined as the time needed to waves propagate from center to the photon sphere radius [84–86]. The echo time can be written as

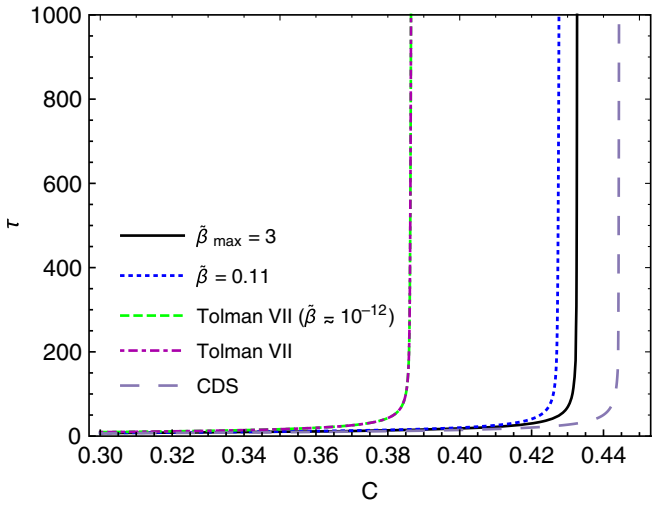

FIG. 7. Echo time τ as a function of compactness. The black line represent maximum parameter, $\tilde{\beta}_{\rm max} = 3$ with $\mathcal{C}_{\rm max} = 0.43$. The blue dashed line denotes the physical condition ($c_s < 1$) with $\mathcal{C} = 0.31$ and $\tilde{\beta} = 0.11$. The green dashed line denotes the TVII model with $\tilde{\beta} = 10^{-12}$, and the magenta dotted-dashed line represents the TVII model solution. The larger dashed line is for the CDS case.

$$\tau_{\rm echo} = \int_0^{3M} \sqrt{-\frac{g_{rr}}{g_{tt}}} dr. \tag{42}$$

Since we have a numerical solution to the metric, it is without a doubt that the result of the echo time has similar behavior. We plot the echo time by varying the compactness as in Fig. 7. As we can see from the figure, the constant density star (CDS) case tends to have infinite echo time near the Buchdal limit. In the TVII model, as described with the green dashed line and magenta dot-dashed line, the appearance of infinity τ is in a region far before the Buchdal limit since it has limited compactness to have finite pressure. The maximum compactness that star can reach is $\mathcal{C}_{\rm max} = 0.38$. When we endowed the nonlocal effect, it is shown that the value of echo time shifted to near the Buchdal limit. It depends on the nonlocal parameter. In this model, we can increase the compactness until $\mathcal{C}_{\rm max} = 0.43$ with $\tilde{\beta}_{\rm max} = 3$. We can infer that the ultracompact star with nonlocal matter can shift the compactness cutoff.

In the following, we investigate the impact of nonlocality that, in the previous discussion, indeed affects the behavior of the effective potential on QNM and gravitational echo wave functions by solving the wave function differential equation in Eq. (39). For the time-independent case, $\Psi(r_*, t) = \psi(r)e^{-i\omega_n t}$, Eq. (39) can be recast into

$$\frac{d^2\psi}{dr_*^2} + [\omega_n^2 - V_{\rm eff}(r)]\psi = 0, \tag{43}$$

where the ω_n is the QNM. The QNM, in general, is a dissipative property of spacetime and plays a crucial role in the form of gravitational wave echo when the stars reach the final stage during a ringdown phase. While the star spans these states, the unstable circular orbit traps the primary signal. In order to obtain the mode, the complex eigenvalue on the time-independent second differential equation shown in Eq. (43) must be solved with the appropriate boundary conditions. From the black hole point of view, since nothing can escape from them, we must employ an inward spherical boundary condition at the black hole horizon

$$\Psi(r_*,t) \approx e^{-i\omega(t+r_*)}, \qquad r_* \to -\infty (r \to 2M). \tag{44}$$

We require a second boundary for the solution to be an outward wave at spatial infinity

$$\Psi(r_*,t) \approx e^{-i\omega(t-r_*)}, \qquad r_* \to \infty (r \to \infty). \tag{45}$$

The case is somewhat different from the ultracompact or compact stars' point of view since they lack the black hole's event horizon. The first boundary condition in Eq. (44) should be replaced by the regularity condition at the center, whereas the second boundary condition in Eq. (45) is unaltered. Therefore, we can implicitly infer that the QNM spectrum for stars is disparate from the black hole. In this paper, we follow Volkel and Kokkotas's [87] procedure to obtain the QNM mode using the Wentzel-Kramers-Brillouin (WKB) approximation. In quantum mechanics, the Bohr-Sommerfeld (BS) rule is a well-known method to receive approximately for the energy spectrum, E_n, of bound states in a potential. With the WKB theory, it is probable to include higher-order correction of BS rule [88]. It means that the WKB approximation is the generalized of BS rule [89]

$$\int_{x_0}^{x_1} \sqrt{E_n - V(x)}dx = \pi\left(n+\frac{1}{2}\right) - \frac{i}{4}e^{2i\int_{x_1}^{x_2}\sqrt{E_n-V(x)}dx}, \tag{46}$$

where x_0 and x_1 are the classical turning point(s) determined by the root of the integrand and also depend on the energy spectrum. The second term in Eq. (46) is the additional term described as the general one for the BS, where x_2 is the third classical turning point on the right side of the potential barrier. For a detailed discussion of this procedure, please see Ref. [87], especially Fig. 1 of this paper. This additional term denotes an exponentially small imaginary part of the energy spectrum, which measures the barrier penetrability. We can simplify further by writing the energy spectrum into $E_n = E_{0n} + iE_{1n}$, where E_{0n} is the real part of the energy whereas E_{1n} is small imaginary energy. Substituting these energy spectrums to the left-hand side of Eq. (46) and matching with the real and imaginary part at the right-hand side of Eq. (46). The results are

$$\int_{x_0(E_{0n})}^{x_1(E_{0n})} \sqrt{E_{0n} - V(x)}dx = \pi\left(n+\frac{1}{2}\right), \tag{47}$$

and

$$E_{1n} = -\frac{1}{2}\left(\int_{x_0(E_{0n})}^{x_1(E_{0n})} \frac{1}{\sqrt{E_{0n}-V(x)}}dx\right)^{-1} \times e^{2i\int_{x_1(E_{0n})}^{x_2(E_{0n})}\sqrt{E_{0n}-V(x)}dx}. \tag{48}$$

Furthermore, we use the well-known analytic fitting potential described below [87]

$$U_Q = U_0 + \lambda_0^2(x-x_{\min})^4 \quad \text{and} \quad U_{\mathrm{BW}} = \frac{U_1}{1+\lambda_1(x-x_{\max})^2}. \tag{49}$$

Both functions above are called the quartic oscillator potential and the Breit-Wigner potential. These two functions depend on U_0, U_1, λ_0, and λ_1 parameters. Then, the value of these parameters is matched with the true effective potential (in tortoise coordinate). The variable U_0 will be the interior of the true potential, whereas the variable U_1 is the one for the maximum of the true potential. Next, λ_1 can be obtained by identifying $V''_{\max}$ on the U_{BW} function, which can be written as $\lambda_1 = -V''_{\max}/2V_{\max}$. The last parameter, λ_0, is not obtained straightforwardly since the minimum does not match the fitting function. The authors of Ref. [87] demand that, for the CDS, the quartic oscillator must be equal to the Regge-Wheeler equation at the surface. Nevertheless, it does not mean we cannot use it for other models. Therefore, in this paper, we use the Regge-Wheeler equation at the surface for TVII and NGTVII models since the effective potentials of both models are shown in Fig. 4 and Fig. 6 are CDS-like. However, we can start to evaluate the energy spectrum by inserting both fitting functions into Eqs. (47) and (48). The detailed calculation of this integral can be seen in Ref. [87]. The solution reads

$$E_{0n} = U_0 + \lambda_0^{2/3}\left[\frac{3\pi}{4\mathcal{K}(-1)}\left(n+\frac{1}{2}\right)\right]^{4/3}, \tag{50}$$

$$E_{1n} = -\frac{\sqrt{\lambda_0}(E_{0n}-U_0)^{1/4}}{4\mathcal{K}(-1)}\mathrm{Exp}\left[4i\sqrt{\frac{U_1-E_{0n}}{\lambda_1}}\mathcal{E}\left(i\sinh^{-1}\left(\sqrt{\frac{U_1}{E_{0n}}-1}\right),\frac{E_{0n}}{E_{0n}-U_1}\right)\right], \tag{51}$$

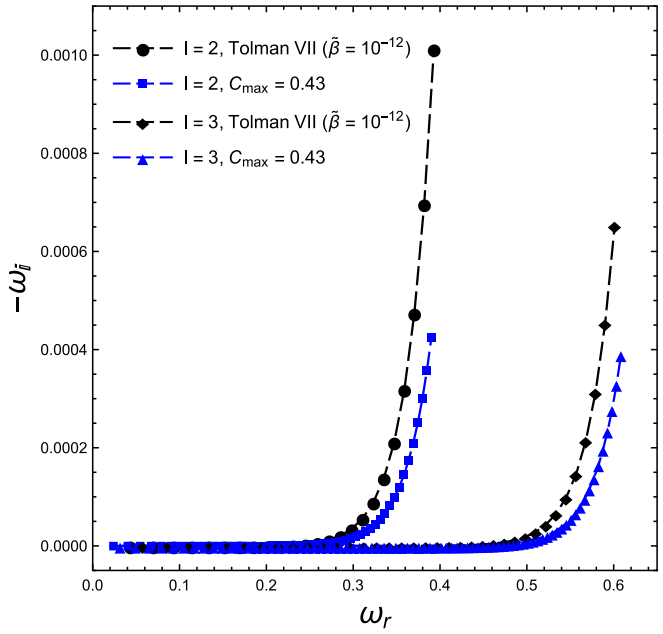

FIG. 8. The QNM $-\omega_i$ vs ω_r with different l and the compactness.

where $\mathcal{K}(a)$ is the complete elliptic integral of the first kind and $\mathcal{E}(a,b)$ denotes the elliptic integral of the second kind [90]. The variable n shown in the Eq. (50) is the overtone number. It is important to note that the expression in Eq. (51) differs with the original one [87], because we use *Mathematica* whereas the authors in Ref. [87] use the *Maple* program, where the definitions of elliptic integrals of both codes are different. Nevertheless, the numerical results of both expressions are the same.[2] Having the spectrum energy in hand, we can match the energy with the complex eigenvalue showed in Eq. (43) which can be written as, $\omega_n = \sqrt{E_n} = \sqrt{E_{0n} + iE_{1n}}$. Splitting the QNM into real and imaginary forms brings us to fully analytic results for all trapped modes in ultracompact stars. The mode can be expressed into $\omega = \omega_r + i\omega_i$, where the real part describes the normal mode of the oscillation and the imaginary part describes the inverse of the damping time, τ_d. The final result of the QNM is shown in Fig. 8. We plot the QNM, $-\omega_i$ vs ω_r, with different l and compactness. All dots (circle, square, diamond, triangle) in the plot represent the overtone number. For TVII model with the aid of the BS fitting procedure, the overtone number for $l = 2$ exceed $n \sim 23$ and for $l = 3$ we have $n \sim 36$, whereas in the NGTVII, the overtone number for the lowest mode is $n \sim 50$ and for $l = 3$ is $n \sim 79$. We can see that the NGTVII model with both $l = 2$ and $l = 3$ can have more overtone numbers than that of the TVII model. From this result, we can also infer that the $l = 3$ mode allowed the ultracompact star to have more trapped mode than the lowest mode ($l = 2$). On the other hand, for both l, the imaginary mode increase as the compactness decrease (from NGTVII to TVII). Therefore, we can infer that the horizonless ultracompact object with nonlocal matter allows the signal for the axial oscillation to be damped longer than the TVII model.

[2]We thank S. Volkel for kindly confirming this issue.

C. Gravitational echoes

In the following, we numerically discuss the gravitational echoes resulting from the perturbed ultracompact star by solving the time-dependent partial differential equation in Eq. (39). Since the differential operator in the equation consists of the second order in t and second order in r_*, the form requires two conditions in the initial data and two conditions at the boundary (at the center and spatial infinity). The conditions are

$$\begin{aligned} &\text{I. } \Psi(r_*, 0) = 0, \\ &\text{II. } \Psi(r_*^c, t) = 0, \\ &\text{III. } \left.\frac{\partial\Psi(t, r_*)}{\partial t}\right|_{t=0} = f(r_*), \\ &\text{IV. } \left.\frac{\partial\Psi(r_*, t)}{\partial r}\right|_{r_*\to\infty} = -\left.\frac{\partial\Psi(r_*, t)}{\partial t}\right|_{r_*\to\infty}. \end{aligned} \tag{52}$$

Conditions I and III are the initial data, whereas II and IV are the boundary conditions. Both initial data denotes the postmerger phase with an initial Gaussian pulse centered at $r_* = r_g$ and with spread σ; $f(r_*) = e^{-\frac{(r_*-r_g)^2}{\sigma^2}}$ [42,91]. Condition III is the condition for the star to be regular at the center, where $r_*^c(r) = r_*(0)$. Lastly, condition IV relates to outgoing waves at spatial infinity. After evaluating numerically, the solution of the differential equation depends on the time and tortoise radius, $\Psi(r_*, t)$. In this discussion, we focus on the time evolution of the signal for the TVII model and the nonlocal one. We investigate further the analysis by depicting the gravitational echoes in Fig. 9. The top picture is the NGTVII's signal, while the bottom is one of the TVII models. The plots use the same models as those of effective potential analysis in Fig. 6. The black line in the Fig. 6 represents the effective potential of NGTVII model with $\mathcal{C}_{\max} = 0.43$ and $\tilde{\beta}_{\max} = 3$. It is shown that the well of the potential is wide, so the signal needs more time to explore the interior. This physical meaning is related to the gravitational echo's plots shown in Fig. 9. As we mentioned earlier, the compactness parameter admitting the causal condition does not exhibit any well in the interior, and thus we can say that the star cannot accommodate the gravitational echoes. It can be proven in the middle panel of Fig. 9 that the behavior of the gravitational echoes in $t > 610$ fluctuates and still have the same pathology until we reach $\mathcal{C} \approx 0.39$ with $\tilde{\beta} = 0.11$. Above this result, the well in the interior of the potential slowly shifts to appear resulting the gravitational echoes. However, it is less interesting since the choices of parameter make

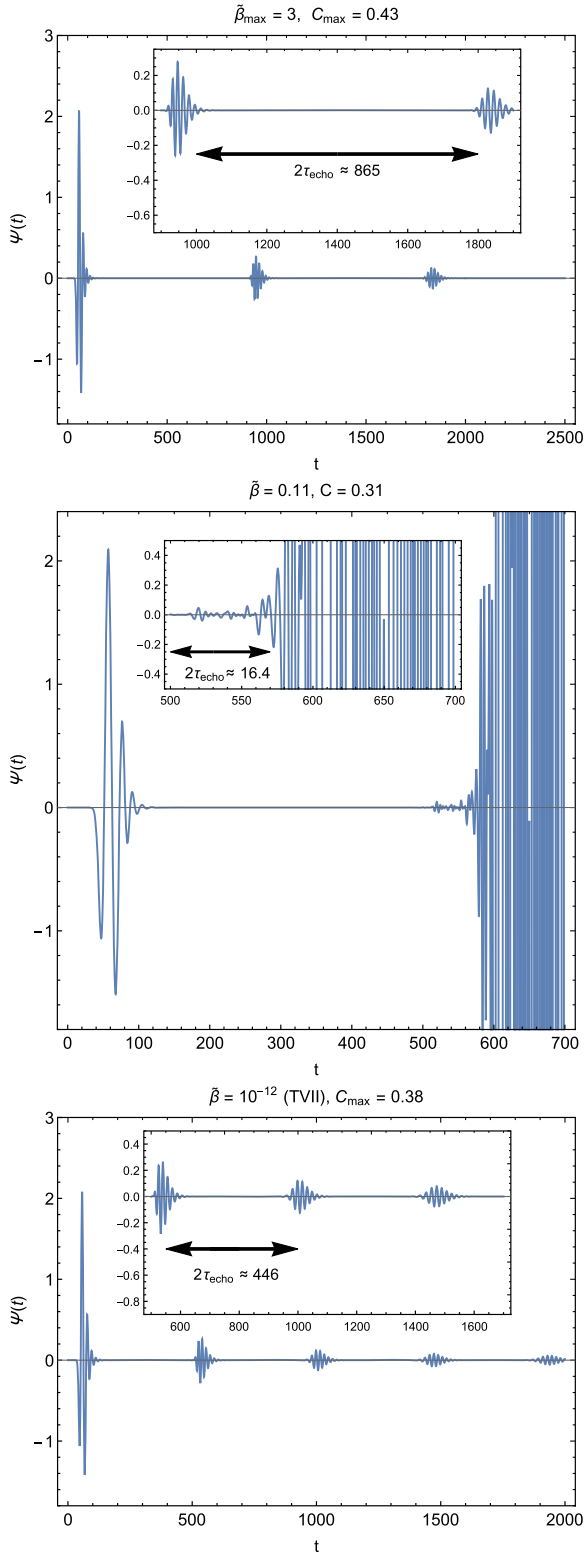

FIG. 9. Gravitational echoes with a different model and compactness. [Top panel] Illustrates the solution with $\mathcal{C}_{\max} = 0.43$ and $\tilde{\beta}_{\max} = 3$, [Middle panel] Illustrates the solution with $\mathcal{C} = 0.31$ and $\tilde{\beta} = 0.11$. [Bottom panel] Illustrates the TVII's gravitational echoes.

the sound of speed and DEC violated. However, from the figures (top and bottom), we can also conclude that the NGTVII's gravitational echoes enable the existence of ultracompact stars to have a longer propagation in the interior than its TVII counterpart.

VI. CONCLUSION

In this work we systematically study the impact of nonlocal gravity of the TVII model (NGTVII) on the properties of the star for an ultracompact star with the compactness range between $0.33 \leq \mathcal{C} \leq 0.44$. The NGTVII model is parametrized by the nonlocal parameters $\tilde{\beta}$ and compactness $\mathcal{C}$. The calculations of the star properties within this model can not be performed analytically anymore. Therefore, we resort to numerical computation. We also investigate the validity of the equation of state of this model by checking its causality condition and its compatibility with energy conditions. Furthermore, we also calculate the echo time, the QNM, and the gravitational echo predicted by this model.

The compactness and the nonlocal parameter characterize the complete numerical solution, and thus we shall elaborate in detail the allowed parameters for NGTVII star to exist. We found that NGTVII can reach $\mathcal{C}_{\max} = 0.43$ with $\tilde{\beta}_{\max} = 3$ which is significantly more compact than that of TVII with $\mathcal{C}_{\max} = 0.38$. However, both maximum compactness does not fit with the causal condition. We have also found that for the relatively small value of $\tilde{\beta}$ and the compactness around, i.e., $\mathcal{C} \approx 0.31$, the speed of sound in this star is subluminal. Consequently, the violation of the DEC in the region near the center is significantly reduced. It means we could use NGTVII as an ultracompact star model. In contrast to the one TVII model with zero density on the surface, the density profile of NGTVII has a different shape and a nonzero value at the surface. It means the density profile has a CDS-like structure. The pressure profile is sensitive to the compactness value. The values of the center pressure can be larger or smaller than the TVII model, depending on the compactness of the stars. However, it is worth noting that for the $\mathcal{C}_{\max}$ case, the pressure near the star's center is higher than that of the TVII model.

The NGTVII's star under axial perturbation turns into a well-known Reggae-Wheeler equation describing three main properties; the eigenfunction, the quasinormal mode, and the effective potential. We also found that the NGTVII's effective potential can be larger and deeper than that of TVII for $\mathcal{C}_{\max}$ case indicating the deceleration of the echo time. The echo time's figure shows decreasing value if the $\mathcal{C}$ value is decreased and vice versa. Furthermore, if we increase the $\tilde{\beta}$, the echo time will be infinite in larger compactness. In the case $\tilde{\beta} = 3$, the echo time for $\mathcal{C} = 0.43$ is larger than that of TVII. Using the effective potential of NGTVII, the QNM and gravitational echo are calculated

using Bohr-Sommerfeld fitting and solving the time-dependent Reggae-Wheeler equation. We have found that for both l, the imaginary part of the mode increase as the compactness decrease. Therefore, we can infer that the ultracompact star of NGTVII allows the signal for the axial oscillation to be damped longer than the TVII model. Furthermore, we can infer that the NGVTII with the maximum compactness and nonlocal parameter values enables the existence of the ultracompact star with more trapped modes than its TVII model counterpart.

ACKNOWLEDGMENTS

We thank S. Volkel and A. Urbano for the discussions related to the numerical QNM and gravitational echo calculation. A. S. thanks I. Belfaqih for the fruitful discussions on the nonlocal gravity.

APPENDIX: DERIVATION FOR INTEGRAL IN EQ. (24)

In this appendix we shall elaborate the detailed calculation for nonlocal effect coupled to the energy density, ρ. We start with the Eq. (24) which can be written as

$$\tilde{\rho} = \mathcal{A}^{-2}(\Box)\rho = \frac{1}{(2\pi)^3}\int_0^\infty ds e^{-s(1+\beta p^2)} \int d^3p \rho(p) e^{i\vec{x}.\vec{p}}. \tag{A1}$$

With the aid of $d^3p = p^2 dp \sin\theta d\theta d\phi$, we can stack the above equation into

$$\tilde{\rho} = \frac{1}{2\pi^2 x}\int_0^\infty ds e^{-s}\int_0^\infty dp p \sin(xp) e^{-s\beta p^2}\rho(p). \tag{A2}$$

To evaluate further, we can employ the Hankel functions and its Fourier transform as

$$\sqrt{k}F(k) = (2\pi)^{3/2}\sqrt{\frac{2}{\pi k}}\int_0^\infty dr r \sin(kr)F(r), \tag{A3}$$

and the result reads

$$\begin{aligned}\tilde{\rho} &= \frac{1}{2\pi^2 x}\int_0^\infty ds e^{-s}\int_0^\infty dp\sqrt{p}\sin(xp)e^{-s\beta p^2}\left[(2\pi)^{3/2}\sqrt{\frac{2}{\pi p}}\int_0^\infty dx' x' \sin(px')\rho(x')\right] \\ &= \frac{2}{\pi x}\int_0^\infty ds e^{-s}\int_0^\infty dx' x'\rho(x')\underbrace{\int_0^\infty dp e^{-s\beta p^2}\sin(px')\sin(px)}_{J},\end{aligned} \tag{A4}$$

where

$$\begin{aligned}J &= \int_0^\infty dp e^{-s\beta p^2}\sin(px')\sin(px), \\ &= \frac{1}{4}\sqrt{\frac{\pi}{s\beta}}[e^{-\frac{(x-x')^2}{4\beta s}} - e^{-\frac{(x+x')^2}{4\beta s}}].\end{aligned} \tag{A5}$$

Substituting into Eq. (A4), we get

$$\begin{aligned}\tilde{\rho} &= \frac{1}{2x\sqrt{\pi\beta}}\int_0^\infty dx' x'\rho(x')\int_0^\infty ds\frac{e^{-s}}{\sqrt{s}}[e^{-\frac{(x-x')^2}{4\beta s}} - e^{-\frac{(x+x')^2}{4\beta s}}], \\ &= \frac{1}{2x\sqrt{\beta}}\int_0^\infty dx' x'\rho(x')(e^{-\frac{|x-x'|}{\sqrt{\beta}}} - e^{-\frac{|x+x'|}{\sqrt{\beta}}}).\end{aligned} \tag{A6}$$

Here, the infinity means the boundary of the star. We also demand that the position should be positive, $x, x' \geq 0$. Hence, we can evaluate the integral and the result is

$$\begin{aligned}\tilde{\rho} = \frac{1}{2\sqrt{\beta}x}\Bigg[&\int_0^x dx' x'\rho(x')e^{-\frac{x}{\sqrt{\beta}}}\left(e^{\frac{x'}{\sqrt{\beta}}} - e^{-\frac{x'}{\sqrt{\beta}}}\right) \\ &+ \int_x^R dx' x'\rho(x')e^{-\frac{x'}{\sqrt{\beta}}}\left(e^{\frac{x}{\sqrt{\beta}}} - e^{-\frac{x}{\sqrt{\beta}}}\right)\Bigg].\end{aligned} \tag{A7}$$

With this equation in hand, we can obtain the final form of the energy density profile. Changing the variable $(x, x') \to (r, r')$ and substituting the Tolman VII density, $\rho(r') = \rho_c[1 - (r'/R)^2]$, we will have

$$\tilde{\rho}(r) = \tilde{\rho}_c e^{-\frac{r+R}{\sqrt{\beta}}}\left[\left(\frac{\sqrt{\beta}}{r} + \frac{3\beta}{rR} + \frac{3\beta^{\frac{3}{2}}}{rR^2}\right)(e^{\frac{2r}{\sqrt{\beta}}} - 1) - e^{\frac{r+R}{\sqrt{\beta}}}\left(\frac{r^2}{R^2} + \frac{6\beta}{R^2} - 1\right)\right]. \tag{A8}$$

[1] S. W. Hawking, Phys. Rev. D **14**, 2460 (1976).
[2] S. D. Mathur, Classical Quantum Gravity **26**, 224001 (2009).
[3] C. Pacilio, Ph.D. thesis, Scuola Internazionale Superiore di Studi Avanzati, 2018.
[4] V. Cardoso and P. Pani, Living Rev. Relativity **22**, 4 (2019).
[5] P. Nicolini, J. Phys. A **38**, L631 (2005).
[6] P. Nicolini, A. Smailagic, and E. Spallucci, ESA Spec. Publ. **637**, 11.1 (2006), https://inspirehep.net/literature/688034.
[7] T. G. Rizzo, J. High Energy Phys. 09 (2006) 021.
[8] S. Ansoldi, P. Nicolini, A. Smailagic, and E. Spallucci, Phys. Lett. B **645**, 261 (2007).
[9] R. Casadio and P. Nicolini, J. High Energy Phys. 11 (2008) 072.
[10] E. Spallucci, A. Smailagic, and P. Nicolini, Phys. Lett. B **670**, 449 (2009).
[11] R. Banerjee, S. Gangopadhyay, and S. K. Modak, Phys. Lett. B **686**, 181 (2010).
[12] D. M. Gingrich, J. High Energy Phys. 05 (2010) 022.
[13] L. Modesto and P. Nicolini, Phys. Rev. D **82**, 104035 (2010).
[14] R. B. Mann and P. Nicolini, Phys. Rev. D **84**, 064014 (2011).
[15] J. R. Mureika and P. Nicolini, Phys. Rev. D **84**, 044020 (2011).
[16] P. Nicolini, A. Smailagic, and E. Spallucci, Phys. Lett. B **632**, 547 (2006).
[17] P. Nicolini and E. Spallucci, Classical Quantum Gravity **27**, 015010 (2010).
[18] P. Nicolini and G. Torrieri, J. High Energy Phys. 08 (2011) 097.
[19] P. Nicolini, Int. J. Mod. Phys. A **24**, 1229 (2009).
[20] R. Banerjee, B. R. Majhi, and S. Samanta, Phys. Rev. D **77**, 124035 (2008).
[21] M. V. Battisti and G. Montani, Phys. Lett. B **656**, 96 (2007).
[22] Y. Shibusa, Int. J. Mod. Phys. A **22**, 5279 (2007).
[23] M. V. Battisti and G. Montani, Phys. Rev. D **77**, 023518 (2008).
[24] K. Nozari and S. Akhshabi, Int. J. Mod. Phys. D **19**, 513 (2010).
[25] M. Bojowald and A. Kempf, Phys. Rev. D **86**, 085017 (2012).
[26] H. Huang, Acta Phys. Sin. **61**, 110403 (2012).
[27] M. Sprenger, P. Nicolini, and M. Bleicher, Eur. J. Phys. **33**, 853 (2012).
[28] M. Isi, J. Mureika, and P. Nicolini, J. High Energy Phys. 11 (2013) 139.
[29] A. F. Ali and A. Tawfik, Adv. High Energy Phys. **2013**, 126528 (2013).
[30] A. N. Tawfik and A. M. Diab, Int. J. Mod. Phys. D **23**, 1430025 (2014).
[31] J. P. Bruneton and J. Larena, Gen. Relativ. Gravit. **49**, 56 (2017).
[32] J. L. Li and C. F. Qiao, Ann. Phys. (Amsterdam) **533**, 2000335 (2021).
[33] P. Nicolini, arXiv:1202.2102.
[34] P. Gaete, J. A. Helayel-Neto, and E. Spallucci, Phys. Lett. B **693**, 155 (2010).
[35] J. R. Mureika and E. Spallucci, Phys. Lett. B **693**, 129 (2010).
[36] J. W. Moffat, Eur. Phys. J. Plus **126**, 43 (2011).
[37] L. Modesto, J. W. Moffat, and P. Nicolini, Phys. Lett. B **695**, 397 (2011).
[38] V. P. Frolov, A. Zelnikov, and T. de Paula Netto, J. High Energy Phys. 06 (2015) 107.
[39] V. P. Frolov, Phys. Rev. Lett. **115**, 051102 (2015).
[40] V. P. Frolov and A. Zelnikov, Phys. Rev. D **93**, 064048 (2016).
[41] V. P. Frolov, Phys. Rev. D **94**, 104056 (2016).
[42] A. Urbano and H. Veermäe, J. Cosmol. Astropart. Phys. 04 (2019) 011.
[43] D. Kramer, H. Stephani, M. A. H. MacCallum, and E. Herlt, *Exact Solutions of Einstein's Field Equations* (Cambridge University Press, Cambridge, England, 1980).
[44] H. A. Buchdahl, Phys. Rev. **116**, 1027 (1959).
[45] S. Hod, Phys. Rev. D **97**, 084018 (2018).
[46] Y. Peng, Eur. Phys. J. C **80**, 755 (2020).
[47] R. C. Tolman, Phys. Rev. **55**, 364 (1939).
[48] W. Kinnersley, *Recent Progress in Exact Solutions*, edited by G. Shaviv and J. Rosen (1975), p. 109.
[49] M. C. Durgapal and G. L. Gehlot, J. Phys. A**4**, 749 (1971).
[50] M. C. Durgapal and P. S. Rawat, Mon. Not. R. Astron. Soc. **192**, 659 (1980).
[51] A. L. Mehra, J. Aust. Math. Soc. **6**, 153 (1966).
[52] N. Jiang and K. Yagi, Phys. Rev. D **99**, 124029 (2019).
[53] N. Jiang and K. Yagi, Phys. Rev. D **101**, 124006 (2020).
[54] C. Posada, J. Hladík, and Z. Stuchlík, Phys. Rev. D **105**, 104020 (2022).
[55] C. Posada, J. Hladík, and Z. Stuchlík, Phys. Rev. D **103**, 104067 (2021).
[56] N. Neary, M. Ishak, and K. Lake, Phys. Rev. D **64**, 084001 (2001).
[57] A. M. Raghoonundun and D. W. Hobill, Phys. Rev. D **92**, 124005 (2015).
[58] A. M. Raghoonundun and D. W. Hobill, arXiv:1601.06337.
[59] S. Hensh and Z. Stuchlík, Eur. Phys. J. C **79**, 834 (2019).
[60] E. Contreras and Z. Stuchlik, Eur. Phys. J. C **82**, 365 (2022).
[61] N. Neary and K. Lake, arXiv:gr-qc/0106056.
[62] L. K. Tsui and P. T. Leung, Mon. Not. R. Astron. Soc. **357**, 1029 (2005).
[63] Z. Stuchlík, J. Hladík, J. Vrba, and C. Posada, Eur. Phys. J. C **81**, 529 (2021).
[64] Z. Stuchlík and J. Vrba, Eur. Phys. J. Plus **136**, 977 (2021).
[65] Y. Y. Ming, Master thesis, The Chinese University of Hong Kong February, 2002.
[66] S. D. Mathur, Fortschr. Phys. **53**, 793 (2005).
[67] L. Buoninfante and A. Mazumdar, Phys. Rev. D **100**, 024031 (2019).
[68] E. Maggio, L. Buoninfante, A. Mazumdar, and P. Pani, Phys. Rev. D **102**, 064053 (2020).
[69] C. Cattoen, T. Faber, and M. Visser, Classical Quantum Gravity **22**, 4189 (2005).
[70] L. Buoninfante, A. Mazumdar, and J. Peng, Phys. Rev. D **100**, 104059 (2019).
[71] G. Panotopoulos, J. Rubio, and I. Lopes, arXiv:2106.10582.
[72] L. Buoninfante, G. Lambiase, G. G. Luciano, and L. Petruzziello, Eur. Phys. J. C **80**, 853 (2020).
[73] L. Buoninfante, G. Lambiase, Y. Miyashita, W. Takebe, and M. Yamaguchi, Phys. Rev. D **101**, 084019 (2020).

[74] J. Boos, J. Pinedo Soto, and V. P. Frolov, Phys. Rev. D **101**, 124065 (2020).
[75] L. Buoninfante, *Nonlocal Field Theories: Theoretical and Phenomenological Aspects* (University of Groningen, Groningen, 2019).
[76] J. Boos, Ph.D thesis, University of Alberta, 2020.
[77] S. Chandrasekhar, *The Mathematical Theory of Black Holes* (The University of Chicago, Chicago, 1984).
[78] P. V. P. Cunha, E. Berti, and C. A. R. Herdeiro, Phys. Rev. Lett. **119**, 251102 (2017).
[79] Y. Kojima, N. Andersson, and K. D. Kokkotas, Proc. R. Soc. A **451**, 341 (1995).
[80] N. Andersson, Y. Kojima, and K. D. Kokkotas, Astrophys. J. **462**, 855 (1996).
[81] K. D. Kokkotas, Mon. Not. R. Astron. Soc. **268**, 1015 (1994).
[82] K. D. Kokkotas and B. F. Schutz, Mon. Not. R. Astron. Soc. **255**, 119 (1992).
[83] M. Leins, H. P. Nollert, and M. H. Soffel, Phys. Rev. D **48**, 3467 (1993).
[84] P. Pani and V. Ferrari, Classical Quantum Gravity **35**, 15LT01 (2018).
[85] M. Mannarelli and F. Tonelli, Phys. Rev. D **97**, 123010 (2018).
[86] D. Kartini and A. Sulaksono, J. Phys. Conf. Ser. **1572**, 012034 (2020).
[87] S. H. Völkel and K. D. Kokkotas, Classical Quantum Gravity **34**, 125006 (2017).
[88] V. S. Popov, V. D. Mur, and A. V. Sergeev, Phys. Lett. A **157**, 185 (1991).
[89] B. M. Karnakov and V. P. Krainov, *WKB Approximation in Atomic Physics* (Springer-Verlag, Berlin, Heidelberg, 2013).
[90] M. Abramowitz and I. A. Stegun, *Handbook of Mathematical Functions with Formulas, Graphs, and Mathematical Tables* (Dover Publications, New York, 1964).
[91] V. Cardoso, S. Hopper, C. F. B. Macedo, C. Palenzuela, and P. Pani, Phys. Rev. D **94**, 084031 (2016).